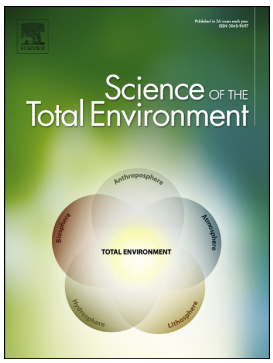

Future atmospheric circulations benefit ozone pollution control in Beijing-Tianjin-Hebei with global warming

Bufan Cao, Zhicong Yin

PII: S0048-9697(20)34167-X

DOI: https://doi.org/10.1016/j.scitotenv.2020.140645

Reference: STOTEN 140645

To appear in: *Science of the Total Environment*

Received date: 27 April 2020

Revised date: 25 June 2020

Accepted date: 29 June 2020

Please cite this article as: B. Cao and Z. Yin, Future atmospheric circulations benefit ozone pollution control in Beijing-Tianjin-Hebei with global warming, *Science of the Total Environment* (2020), https://doi.org/10.1016/j.scitotenv.2020.140645

Future Atmospheric Circulations Benefit Ozone Pollution Control in Beijing-Tianjin-Hebei with Global Warming

Bufan Cao[1] and Zhicong Yin [123]

[1]Key Laboratory of Meteorological Disaster, Ministry of Education / Joint International Research Laboratory of Climate and Environment Change (ILCEC) / Collaborative Innovation Center on Forecast and Evaluation of Meteorological Disasters (CIC-FEMD), Nanjing University of Information Science & Technology, Nanjing 210044, China

[2]Southern Marine Science and Engineering Guangdong Laboratory (Zhuhai), Zhuhai, China

[3]Nansen-Zhu International Research Centre, Institute of Atmospheric Physics, Chinese Academy of Sciences, Beijing, China

Corresponding author: Zhicong Yin (yinzhc@163.com)

Address: No. 219 Ningliu Road, Pukou District, Nanjing University of Information Science & Technology, Nanjing 210044, China

Tel.: (+86) 13655161661

Abstract. Surface ozone pollution has become increasingly serious in recent years. Ozone pollution will damage human health and reducing social productivity in China. Basing on an ozone weather index (OWI) that captured the effects of climate on the ground-level ozone, large ensemble simulations by the Community Earth System Model were introduced to project future impacts of atmospheric circulation on

ozo[illegible]vill favour the control of ozone pollution in Beijing-Tianjin-Hebei region. The OWI decreased overall during the 21st century, which was nearly ignored by other studies on ozone projections. The OWI decrease was mainly due to the increase in regional precipitation and partly due to the changes of wind and the temperature difference between 200 hPa and lower-troposphere. The increased total precipitation in the 21st century, mainly due to the increase in convectional precipitation, weakened the production of surface ozone by its shading effect (related to more cloud cover) and wet deposition impact. During 2061–2100, the South Asia High will move southward, and the west Pacific subtropical high will shift eastward; thus, the convergence of water vapour will mainly occur in South China. Consequently, the large-scale precipitation will decrease over northern China. However, because of climate warming, the increase in specific humidity in Beijing-Tianjin-Hebei region (BTH) will enhance convectional precipitation, which will be more than 4 times the decrease in large-scale precipitation.

1 Introduction

Ozone pollution will damage not only human health but also the social economy. With an approximately 20% decrease in ozone, work time per day will increase by 0.1 h and save 50 billion Yuan in health expenditures in China (Xie et al., 2019). Most cities in East China have exceeded the O_3 pollution level of the Chinese National Ambient Air Quality Standard (i.e., the maximum daily average 8 h concentration of ozone (MDA8) > 160 μg m^{-3}) (Li et al., 2018). The highest MDA8, indicating the most severe surface ozone pollution, are observed in North China (Li et al., 2018; Yin et al., 2019a). As one of the largest mega-city clusters in China, Beijing-Tianjin-Hebei (BTH) exhibited an obvious increasing trend of the summer mean MDA8 from 2013 to 2017 (Li et al., 2018), which became the main air pollution in this region in summer (Wang et al., 2017) and resulted in increasing premature moralities (Xie et al., 2019).

cal conditions. Many researchers have discussed the effects of precursor emissions. Increasing emissions of nitrogen oxides (NO_x) and volatile organic compounds (VOCs) are responsible for the increase in surface ozone in Beijing from 2006 to 2016 (Chen et al., 2018). Compared with NO_x, VOCs have played more important roles in increasing ozone in North China in recent years (Li et al., 2019). Some studies pointed out that climate has significant effects on the surface ozone concentration. Photochemical precursors and meteorological parameters were used to predict tropospheric ozone as predictors (Mehdipour et al., 2017; Yin et al., 2020). Meteorological factors, such as cloud cover, surface air temperature and specific humidity, have strong relationships with ozone formation (Melkonyan et al., 2012; Kim et al., 2014). Except for the three meteorological factors mentioned above, other local weather conditions, such as regional anomalous southerlies near the surface, precipitation and regional relative humidity, are closely connected to the local ground-level ozone in North China (Yin et al., 2018). Surface pressure and planet boundary height are also thought to be important factors (Chen et al., 2018; Wang et al., 2013). Temperature is the key meteorological factor that has an influence throughout almost the whole year (Chen et al., 2020). The sharp increase in ozone across China was partially attributed to changes in temperature, solar radiation and relative humidity (Chen et al., 2020). Wind, humidity and daily solar radiation exerted major effects on ozone in winter (Chen et al., 2020). A multiple linear regression model was used to describe the meteorological conditions during the ozone variation in BTH. According to their relationship with MDA8, the top three predictors are daily maximum temperature, meridional wind speed at 10 m and relative humidity, which were used to establish the model (Li et al., 2018). The ozone weather index (OWI) was adopted to simulate the features and variations in ozone pollution in North China via high correlations and the physical mechanisms between meteorological factors and ozone observations (Yin et al., 2019b,c). A close connection was found between North China surface ozone and the Eurasian teleconnection pattern. Increased solar radiation and high air temperatures during the

North China transported surrounding O_3 precursors to superpose local emissions. Furthermore, the preceding May Arctic sea ice could explain approximately 60% of the interannual variability in O_3-related weather conditions (Yin et al., 2019c).

There are some researches about pollution change under global warming (Wang et al., 2019; Lee et al., 2015; Wang et al., 2013; Kim et al., 2014; Mulenga et al., 2019; Mahmud et al., 2020). Several studies projected ground-level ozone pollution in China.. Most of the studies illustrated sharply increasing trends in the mid-21st century over eastern China (Wang et al., 2019; Lee et al., 2015; Wang et al., 2013; Kim et al., 2014). Lee et al. (2015) projected the summertime ozone concentration under multiple Intergovernmental Panel on Climate Change Special Reports on Emissions Scenarios and showed that surface ozone in North China will increase in the 2050s under all paths except B1 and decrease in the 2090s under all paths except A2. Furthermore, surface ozone will increase in 2050 under most representative concentration pathway (RCP) scenarios except RCP8.5 (Kim et al., 2014). This increase was attributed to the changes in anthropogenic emissions, which will change climate effects on the sensitivity of surface ozone to emissions (Wang et al., 2013). Most of these projections were based on the different anthropogenic emissions and mostly analyzed the variations in surface ozone on a global or a country scale. Few of the studies extended the projection period to the end of the 21st century. Large-scale projections result in uncertainties when applying their results in a small area such as BTH. Some studies showed an increase centre in BTH (Kim et al., 2014). However, other studies showed that there was a boundary between the increasing ozone region and decreasing ozone in the BTH area (Wang et al., 2013). Furthermore, most of the previous studies focused on ozone change by assessing the effects of emissions. The influences of changes in meteorological conditions on ozone at the end of the 21st century have not been investigated in detail, which largely limits understandings of real changes in ozone pollution in the future and the associated reasons.

the OWI built in our research before (Yin et al., 2019b), OWI was modified to be suitable for numerical climate model, e.g., Community Earth System Model -Large Ensemble data. In this research, section 2 introduce the data and methods (see flowchart in Figure S1). Section 3 shows the historical performance of ozone weather index during 1979-2018. Section 4 shows future variations in OWI. Section 5 is conclusions and discussions.

2 Data and methods

2.1 Data set

Public hourly O_3 concentration data since May 2014 are available online (http://beijingair.sinaapp.com/). The national ozone data are mostly observed by urban stations and are updated daily from the national urban air quality real-time release platform of the China Environmental Monitoring Headquarters. The MDA8 was calculated as the maximum 8-h running average from 00:00 to 23:00 every day. By eliminating stations with more than five percent missing data, 77 stations were chosen from 90 stations in Beijing-Tianjin-Hebei. There are 12 sites in Beijing, 14 sites in Tianjin, and 51 sites in 11 different cities in Hebei Province. Sporadic missing data were filled by cubic spline interpolation. Successive missing data (from 15 July 2014 to 24 July 2014 at all stations) were dropped. Therefore, the measured ozone in BTH was represented by the mean MDA8 at 77 stations.

The 1°×1° ERA-Interim reanalysis dataset from 1979 to 2018 was used here, including the air temperature, zonal and meridional wind, relative humidity, specific humidity at 850 hPa, downward solar radiation at the surface, low and medium cloud cover and precipitation (Dee et al., 2011).

The Community Earth System Model (CESM) Large Ensemble Project (CESM-LE) is a publicly available dataset of climate model simulations, including a 40-member ensemble of fully coupled CESM1 simulations for the period 1920-2100 (Kay et al., 2015). Each member is subject to the same

rad tly different initial atmospheric state. This research used monthly large-scale precipitation and convective precipitation, air temperature at 850 hPa and 200 hPa, geopotential height (Z) at 850 hPa, 500 hPa and 100 hPa, zonal wind and relative humidity at 850 hPa, wind, vertical velocity, and specific humidity from the surface to 200 hPa at a resolution of 1.5°×0.94°.

The fifth phase of the Coupled Model Intercomparison Project (CMIP5) is widely adopted to help to deepen people understanding on climate change (Tylor et al., 2012). 15 models were introduced to verify the conclusion from CESM-LE. They are under same radiative forcing scenario with CESM-LE. Specific model information is shown in Table S2. All model data was interpolated into a resolution of 1.0°×1.0° with Climate Data Operators.

2.2 Methods

With global warming, the geopotential height increased throughout the layer during the 21st century; thus, the eddy geopotential height was taken to determine the relative change in geopotential height (Huang et al., 2015, Wei et al., 2014).

$$\text{Eddy geopotential height}_{i,j} = Z_{i,j} - \text{Zonal mean } (Z_i)$$

where i and j are the latitude and longitude, respectively.

Meteorological conditions affecting air pollution could be represented by several key synoptic systems (Liao et al., 2019; Cai et al., 2017). Cai et al. (2017) fitted a haze weather index by evaluating the relationship between $PM_{2.5}$ and local weather conditions and then projected future haze weather conditions under RCP8.5. They pointed out that weather conditions conducive to severe haze in Beijing were more frequent under climate change. Yin et al. (2019b) calculated the OWI by fitting meteorological data with Shangdianzi ozone observations. We modified the OWI to be adopted the numerical climate models and match the BTH area. An modified OWI was calculated as:

$$\text{OWI} = \text{normalized } (\text{DTI} + \text{V850pI} - \text{V850nI} + \text{PI})$$

Pa

(T200: 110°E–130°E, 35°N–50°N) were used to calculate DTI. DTI, daily meridional wind over two different regions (V850nI: 92.5°E–100°E, 40°N–50°N; V850pI: 105°E–112.5°E, 32.5°N–42.5°N) at 850 hPa, and total precipitation (PI: 112.5°E–120°E, 37.5°N–42.5°N) were used to fit this modified OWI. These related factors mainly represent three important weather systems (Figure S2). The temperature difference between 850 hPa and 200 hPa (Figure S2a-d) is related to sunny-hot days, which favour photochemical reactions (Yin et al., 2019b). The temperature at 200 hPa was also linked to an anomalous anticyclone high in the atmosphere. The correlation coefficient of the temperature difference between the two layers with the measured MDA8 is 0.52 (Table 1). An anomalous cyclone is located northwest of BTH, and an anomalous anticyclone is located over BTH (Figure S2e-f). This distribution is associated with the downward flow in the lower atmosphere, which favours ozone pollution (figure omitted). The difference between these two meridional winds indicates the dynamic effects of atmospheric circulation in the lower troposphere. V850pI present the south anomalies which shared by anomaly cyclone to the north-west of BTH and anomaly anticyclone to the east of BTH. V850nI was used to strengthen capturing cyclonic curvature by representing the north-west branch of the anomaly cyclone. The correlation coefficient between atmospheric circulation and measured ozone is 0.34, which is above the 99% confidence level (Table 1). It is higher than each single of them (V850pI: 0.18; V850nI: −0.26). Observed decreasing trend of wind (−0.27 per decade) were successfully reproduced in CESM-LE (−0.26 per decade) from 1984 to 2018. Precipitation is also an important factor (-0.40, above the 99% confidence level). Correlation coefficients between total precipitation and medium and low cloud cover is 0.75 (above 99% confidence level). That means precipitation index can represent both precipitation and cloud cover impact, which is related to less solar radiation but full cloud cover (Figure S2g-j). Wet deposition also clears away the stock of ozone pollution and its precursors in the air.

The daily OWI calculated from the daily ERA-Interim datasets (OWI-ERA) is highly related to the measured MDA8 (Figure 1a). The correlation coefficient between the two is 0.62 during 2014–2018 (451 daily samples). The daily variation in OWI-ERA is similar to the measured ozone. The ozone concentration is mostly largest in June and decreases monthly from July to August. On the monthly time scale, the correlation coefficient is 0.78 (above the 99% significance level); thus, the OWI-ERA could also capture the monthly variations in measured ozone pollution (Figure 1b). Figure 1c shows the distribution of the correlation coefficients between the daily MDA8 and OWI-ERA from 2014 to 2018, which were above the 99% significance level at all sites.

The purpose of this study is to project the meteorological conditions associated with ozone pollution at the end of the 21st century; thus, we also calculated OWI-LE from CESM-LE datasets and first verified its performance in the historical period (HIST, 1979–2018). On the one hand, when more simulation members are used in the ensemble mean, the external forcing would account for an increased proportion, and the projections would be more reliable (Lu et al., 2019). On the other hand, many members would excessively exclude the internal variability in the climate system (Lu et al., 2019). To find a better balance, we calculated the impacts of the number of members on the internal variance. Consistent with Lu et al. (2019), the simulations converged rapidly when the number of members used was more than 5 and plateaued when the number was more than 20 (Figure S3). Finally, according to the correlation coefficients with OWI-ERA, the OWI-LE was established with 23 members. The 23 members could balance the need for convergence and the need for a high correlation between CESM-LE simulations and reanalysis data. This result means that our OWI-LE will be as similar as possible to the results based on all 40 members, with correlation coefficients of 0.94 between them over 122 years.

on coefficient of 0.48 (above the 99% significance level) during 1979–2018 between them. OWI-LE also have the same mathematical symbol in 72.5% summers, relative to OWI-ERA (Figure 2). Over the past 40 years, OWI-ERA showed an insignificant downward trend (i.e., 0.031). This trend was also found in OWI-LE with similar slope rates (i.e., 0.023, Fig 2). Furthermore, both OWI-ERA and OWI-LE have sectional upward trends during 1979–1983, 1988–1992, 1998–2005 and 2014–2018. There are also comparable downward trends during 1983–1988, 1992–1998 and 2005–2014 in both of them (Figure 2) The increasing trend from 2014 to 2018 is also precisely consistent with that of measured ozone (Figure 2). Both the long-term and the staging trends were quite similar, indicating the good performances of the CESM-LE simulations in reproducing the decadal-multi decadal variations in ozone-related meteorological conditions.

In addition to the reproduction of trends, the related physical mechanisms were also revealed in the CESM-LE simulations. Composites of regional weather conditions successfully capture the meteorological systems related to ozone accumulation (Figure 3). A large-scale positive temperature difference between 850 hPa and 200 hPa was found in ERA-Interim over BTH (Figure 3a), which presents sufficient local solar radiation and an anomalous anticyclone over BTH (Yin et al., 2019 a,b). Consistently, this positive temperature difference also occurred in the CESM-LE simulations (Figure 3b). The anomalous anticyclonic circulations over BTH resulted in reduced cloud cover and corresponded to warmer surface air temperature (Figure 3c). Although the anticyclonic circulations shifted southward and became weaker, the southerlies to the west of BTH, which prevent the intrusion of clear and cold air from the north, are found in the CESM-LE simulations (Figure 3d). Reduced cloud cover and descending motions were unfavourable to rainfall over BTH. The characteristics of decreased rainfall days are also presented (Figure 3e, f), indicating weakened wet deposition and strengthened photochemical reaction. This situation will lead to more ozone production by photochemical reactions

but ure via CESM-LE simulations.

4 Future variations in OWI and physical mechanisms

4.1 Future variations in OWI

Since 2030, meteorological conditions have become increasingly beneficial for controlling ozone pollution, i.e., the OWI-LE values are persistently negative (Figure 4c). There are two sharp drops in OWI-LE around the 2030s and around the 2060s according to the 11-year running average. The value almost maintains a similar level in the rest of the 21st century before the 2080s. The amplification of OWI-LE also strengthened in the future (Figure 4a). The standard deviation of OWI-LE in the late 21st century increases, which means that ozone weather conditions will change over a large range in the future. The mean OWI-LE is −1.73 in the mid-21st century (2020–2059), and the OWI-LE is close to the negative area in Figure 4a. The decreasing trend becomes more significant in the last 40 years of the 21st century (Late-21C), with a mean OWI-LE value of −4.27. Illustrated by the frequency of OWI-LE, the OWI-LE moved to negative values in the 21st century (Figure 4a). This result means that meteorological conditions were more unfavourable to ozone production in BTH during the late 21st century.

Meteorological conditions change largely in the 21st century under RCP 8.5. The differences in climate conditions between Late-21C and HIST are significant in most areas of East Asia. The eddy geopotential height at 850 hPa decreases over most of the East Asian continent. Wind over BTH became more cyclonic in the lower atmosphere during Late-21C (Figure 5a), indicating more active convections in the lower atmosphere. Specific humidity increased from the surface to the high troposphere (Figure 5b). The convectional precipitation in East Asia increased (Figure 5c). However, large-scale precipitation decreased approximately north of 31°N. Statistically, the increase in convectional

pre[illegible]tal precipitation increased during Late-21C compared to HIST precipitation (Figure 5c).

To determine the reasons for the negative OWI-LE in Late-21C, its components (sub-index) were analysed, which show different varying features (Figure 6a). The decrease in OWI was mainly due to an increase in precipitation (Figure 6d). This decrease also comes from temperature differences and cyclonic circulations in the lower atmosphere (Figure 6b, c). The wind index (i.e., V850pI–V850nI) decreases before 2080 and then increases (Figure 6c). The change in wind is responsible for the increase in OWI-LE over the last 20 years (Figure 6c). The temperature difference between two layers was used to describe the impacts on photochemical reactions and dynamic anticyclones in the high troposphere over BTH (Yin et al., 2019a). Although the temperature in the atmosphere significantly increased with global warming (Figure S4 a, b), the trends of T200 and T850 counteracted when calculating the OWI (Figure 6b).

The negative values of OWI (mean value =−2.03) can also be simulated without PI during Late-21C (Figure 5b, c). It is clear that the change in precipitation shows a more dramatic decreasing trend and plays a more important role than the other two sub-indexes (Figure 6). As mentioned above, the increase in total precipitation mainly comes from convectional precipitation. A decline in large-scale precipitation reduces the increasing trend of total precipitation. The changes in precipitation are similar to those in specific humidity and relative humidity in the lower atmosphere. The specific humidity at 850 hPa increased, but the relative humidity decreased at 850 hPa (Figure S4). To explore the linkages between the two kinds of precipitation and humidity, we calculate the correlation coefficients between them from 1979 to 2100 (Figure 7). High specific humidity significantly corresponded to an increase in convectional precipitation (Figure 7a). However, high relative humidity favours large-scale precipitation in BTH (Figure 7b). According to the Clapyron-Clausius equation, a high air temperature will enhance the ability of the atmosphere to retain water. Global warming will increase the specific humidity but

dec ınd

contributes to increasing convectional precipitation and decreasing large-scale precipitation.

4.2 Changed precipitation and associated physical mechanisms

What happens in the atmospheric circulations that are linked to the change in precipitation? The declines in large-scale precipitation are attributed to the eastward shift of the western Pacific subtropical high and the southward shift of the South Asia High (SAH) (Figure 8). To clarify the north-south shift of the SAH, we calculate the I_{ns} as the difference in the area-averaged eddy geopotential height at 100 hPa over in the region of 27.5°–32.5°N, 50°– 100°E and the region of 22.5°–27.5°N, 50°–100°E (Xu et al., 2017). Similar to many previous studies, the SAH will shift to the south during the 21st century with global warming (Qu et al., 2016). The I_{ns} mean value was 31.23 during 1979–2018 and will be 22.61 from 2061 to 2100. Combined with the southward shift of the SAH, the eastward shift of the western Pacific subtropical high (Figure 8) and anomalous cyclone over southern China (Figure 5a) weaken the large-scale water vapour flux to northern China (Figure 9). Thus, more water will be detained in southern China. The correlation coefficients between Ins and relative humidity over BTH at 850 hPa were calculated. This value is 0.56 during 1979–2100, which is above the 99% confidence level, and illustrates that the southward shift of the SAH will decrease relative humidity over the BTH area. This result explains why large-scale precipitation increases in southern China and decreases in northern China (Figure 5c).

We regressed the large-scale precipitation onto omega at 850 hPa and then subtracted it from the total simulated omega to clarify the vertical motions related to convective precipitation. We found that the southward shift of the SAH exhibited a strong relationship with anomalous vertical uplift at 850 hPa over BTH (Figure 9). As mentioned above, with global warming, the specific humidity will increase in the atmosphere (Lu, 2013). The enhanced ascending motions associated with the changes in the SAH and increased specific humidity in a warming environment jointly strengthened the convectional

pre

5 Conclusions and discussions

In this research, the CESM-LE data were introduced to project future ozone weather conditions in BTH, which was not focused on in previous research. A high emission path, RCP 8.5, was taken as the possible future emission scenario. During the historical period, OWI calculated from CESM-LE perform well in reproduction of long-term trend and sub-trends in reanalysis data. Future atmospheric circulation conditions favour the control of ozone pollution in the BTH region. OWI will decrease −4.27 in late 21st Century. The OWI without precipitation was also calculated. It will decrease in the 21st Century, with a mean value of −2.03 from 2061 to 2100.Thus, the OWI decrease is mainly due to regional precipitation changes. Temperature difference between 850 hPa and 200hPa and wind at 850 hPa partially contribute to part of its decrease. Because South Asia High will move to south ward and Western Pacific Subtropical High will move to eastward under global warming, large-scale precipitation will decrease in the future. Although large-scale precipitation will decrease in 21st Century, change of convective precipitation is 4 times large-scale precipitation reduction. Its increase comes from increasing specific humidity and upward anomalies related to southward shift of South Asia High under global warming. Thus, total precipitation will increase in the future. Enhanced shading (related to cloud cover) and wet deposition effect of precipitation will unfavour ozone pollution. Furthermore, CMIP5 data set were also introduced to our research and consistent results (including the change of precipitation, cloud and OWI) were obtained (Figure S6).

In this study, we used precipitation instead of cloud cover because of their highly cross-correlations. We also modified OWI by taking both information of precipitation and cloud cover into it. Some important points should be noticed. Without convective precipitation, OWI performance will significantly get worse (Table S3). Climate model show large uncertainties on simulating about cloud

cov ina

(Li et al., 2017). With calculating cloud cover into OWI, the highest correlation coefficient is 0.41 (above 95% confidence level) and the highest same mathematical symbol is 67.5% (Table S3). Both of them are worse than OWI we adopted. Even so, projection was also made of taking both cloud cover and precipitation into OWI. It also show changes of atmospheric circulations will benefit ozone control (Figure S7).

Previous ozone pollution projections mainly simulated the ozone concentration by driving atmosphere chemical pollution models (Lei et al., 2012; Wang et al., 2013; Kim et al., 2014; Lee et al., 2015). Few studies have explained atmospheric circulation changes and its effect on ozone weather conditions in north China. It led to uncertainties in projecting impacts of atmospheric circulation on regional ozone pollution. Some of the studies pointed out that climate change will lead to an increase in surface ozone concentration in eastern China (Wang et al., 2013; Kim et al., 2014). However, Wang et al. (2013) thought that the centre of ozone increase was located in southeastern China, while Kim et al. (2014) found that the centre was located in northeastern China. It is difficult to say whether there will be an obvious change in the ozone concentration because BTH is located at the junction of areas that exhibit increases and decreases (Wang et al., 2013; Kim et al., 2014). According to our research, changes in weather conditions related to ozone pollution will not favour ozone increases in BTH. Compared with previous studies, we could make an inference that ozone pollution will become more serious if there is no inhibition of meteorological factors.

At the global or continental scale, correlations were illustrated between global mean climate factors and the global mean ozone concentration (Kim et al., 2014). At this scale, it is reasonable that precipitation was not indicated as an important factor in the ozone projection. However, it is important to consider precipitation when talking about ozone pollution over a small area. The increase in water vapour in 2050 will accelerate the destruction of O_3 in low NO_x regions (Wang et al., 2013). In areas

wi ved,

the surface O_3 concentration will decrease in the 2050s (Wang et al., 2013). This finding also means that the effect of climate on ozone pollution will change with anthropogenic emissions and become nonlinear. The effect of regional weather conditions in recent years is smaller than that in the future because of increased greenhouse gas concentrations (Lee et al., 2015). This research aimed to project the climate over a small but extremely important region, and the projections possibly included some uncertainties. We tried different statistical approaches and different combinations of meteorological sub-indexes and reached consistent results, which indeed reduced the uncertainties. Research to subdivide the roles of climate change and variability under different emission levels should be conducted in the future to better understand the effect of climate on surface ozone pollution.

***Data availability*.**

CESM Large Ensemble Datasets for this research are available from the following in-text data citation references: Kay et al., 2015. The CMIP5 Data is now available through the portal, on the page http://esgf-node.llnl.gov/. ERA-Interim datasets for this research are available from the following in-text data citation references: Dee et al., 2011. Public hourly O3 concentration data since May 2014 are available online (http://beijingair.sinaapp.com/).

Author contribution.

ZY designed this research. BC and ZY plotted figures and conducted the analysis. BC and ZY finished this manuscript.

Competing interests.

The authors declare that they have no conflict of interest.

***Acknowledgements*.**

This research has been supported by National Natural Science Foundation of China (grant nos.

team.

References

Cai, W. J., Li, K., Liao, H., Wang, H. J., & Wu, L. (2017), Weather conditions conducive to Beijing severe haze more frequent under climate change. Nature Climate Change, 2017, 7(4), 257–262.https://doi.org/10.1038/nclimate3249

Chen, H. P., Sun, J. Q., & Xia, X. L. (2012), The Projection and Uncertainty Analysis of Summer Precipitation in China and the Variations of Associated Atmospheric Circulation Field. Climatic and Environmental Research (in Chinese), 17(2), 171–183, DOI:10.3878/j.issn.1006–9585.2011.10137.

Chen, Z., Zhuang Y., Xie X., Chen, D., Cheng, N., Yang, L., & Li, R. (2019), Understanding long-term variations of meteorological influences on ground ozone concentrations in Beijing During 2006–2016. Environmental Pollution, 2019, 29–37. https://doi.org/10.1016/j.envpol.2018.10.117

Chen, Z., Li, R., Chen, D., Zhuang Y., Gao, B., Yang, L., & Li, M. (2020), Understanding the causal influence of major meteorological factors on ground ozone concentrations across China. Journal of Cleaner Production, https://doi.org/10.1016/j.jclepro.2019.118498

Dee, D. P., Uppala, S. M., Simmons, A. J., Berrisford, P., Poli, P., Kobayashi, S., Andrae, U., Balmaseda, M. A., Balsamo, G., Bauer, P., Bechtold, P., & Beljaars, A. C. M. (2011), The ERAInterim reanalysis: configuration and performance of the data assimilation system, Quarterly Journal of the Royal Meteorological Society, 2011, 137, 553–597, DOI: 10.1002/qj.828,.

Kate M., Mark D Z., Stephen A K., Celine B., Peter C., Charles D., Benjamin D S. & K. E. Taylor (2015). External Influences on Modeled and Observed Cloud Trends. Journal of Climate, 28(12), 4820-4840. DOI: 10.1175/JCLI-D-14-00734.1

Kay, J. E., Deser, C., Phillips, A. , Mai, A., Hannay, C., Strand, G., Arblaster J. M., Bates S.

C., D. M., Lindsay, K., Middleton, A., Munoz, E., Neale, R., Oleson, K. W., Polvani, L. M., & Vertenstein, M. (2015), The Community Earth System Model (CESM) Large Ensemble Project: A Community Resource for Studying Climate Change in the Presence of Internal Climate Variability, Bulletin of the American Meteorological Society, DOI:10.1175/BAMS–D–13–00255.1, 96, 1333–1349

Kim, M. J., Park, R. J., Ho, C. H., Woo, J. H., Choi, K. C., Song, C. K., & Li, J. B. (2014), Future ozone and oxidants change under the rcp scenarios. Atmospheric Environment, 2014, 101, 103–115. https://doi.org/10.1016/j.atmosenv.2014.11.016

Huang, Y. Y., & Li X. F. (2015), The interdecadal Variation of the western Pacific subtropical high as measured by 500 hPa eddy geopotential height. Atmospheric and Oceanic Science Letters. 2015, 8, 371–375. DOI: 10.3878/AOSL20150038

Lee, J. B., Cha, J. S., Hong, S. C., Choi, J. Y., Myoung, J. S., Park, R. J., & Woo, J. H. (2015), Projections of summertime ozone concentration over East Asia under multiple IPCC SRES emission scenarios. Atmospheric Environment, 2015, 106:335–346. https:/doi.org/10.1016/j.atmosenv.2015.02.019

Lei, H., Wuebbles, D., J., & Liang, X. Z. (2012), Projected risk of high ozone episodes in 2050. Atmospheric Environment, 2012, 59(59), 567–577. https://doi.org/10.1016/j.atmosenv.2012.05.051

Li, D. H., Zou, l. W., & Zhou, T. J. (2017), Regional model estimation of extreme events in China under the global 1.5℃ temperature rise. In Chinese, Progress in earth science. 2017, (4). DOI: 10.11867 / j.issn.1001-8166. 2017.04.0446

Li, J., Zhu, Z., & Dong, W. (2017). Assessing the uncertainty of CESM-LE in simulating the trends of mean and extreme temperature and precipitation over China. International Journal of Climatology, 37(4), 2101-2110. https://doi.org/10.1002/joc.4837

Li, K., D. J. Jacob, Liao, H., Zhu, J., Shah, V., Shen, L., Bates, K. H., Zhang, Q., & Zhai, S. (2019), A

two ure

Geoscience. https://doi.org/10.1038/s41561-019-0464-x.

Li, K., D. J. Jacob, Liao, H., Shen, L., Zhang, Q. & Bates, K. H. (2018), Anthropogenic drivers of 2013-2017 trends in summer surface ozone in China, Proceedings of the National Academy of Sciences, 116(2), 422–427, DOI:10.1073/pnas.1812168116.

Liu Y., Wang T., Worsening urban ozone pollution in China from 2013 to 2017 Part1: The complex and varying roles of meteorology. Atmospheric Chemistry and Physics, 20, 6305–6321, 2020, https://doi.org/10.5194/acp-20-6305-2020

Lu, A. G. (2013), The influence of global warming on the change of regional relative humidity in China. Ecology and Evironmental Sciences. In Chinese, 2013 (22). DOI : 10.16258/j.cnki.1674-5906.2013.08.008

Lu, J. W., Zhou, T. J., Huang, X., Hang, W. X., & Zou, L. W. (2020), Comparative study on estimation methods of internal variability of surface temperature. Atmospheric science, 44(1): 105–121, DOI: 10.3878/j.issn.1006–9895.1901.18235.

Mahmud A. I. & Hasibul H. (2020). Generation of IDF Equation from Catchment Delineation Using GIS. Civil Engneering Journal. DOI: 10.28991/cej-2020-03091490

Mehdipour, V., & Memarianfard, M. (2017) Application of support vector machine and gene expression programming on tropospheric ozone prognosticating for Tehran metropolitan, Civil Engineering Journal 3(8):557-567, DOI: 10.28991/cej-030984

Melkonyan, A., & Wagner P. (2013), Ozone and its projection in regard to climate change. Atmospheric Environment (2013): 287–295. DOI: 10.1016/j.atmosenv.2012.10.023

Mulenga, D. & Siziya, S. (2019) Indoor Air Pollution Related Respiratory III Health, a Sequel of Biomass Use, SciMedicine Journal, https://dx.doi.org/10.28991/SciMedJ-2019-0101-5

Qu, X., & Huang, G. (2016), The global warming-induced south asian high change and its uncertainty.

Taylor, K.E., R.J. Stouffer, G.A. Meehl (2012): An Overview of CMIP5 and the experiment design." Bull. Amer. Meteor. Soc., 93, 485-498, DOI:10.1175/BAMS-D-11-00094.1, 2012.

Wang, P., Chen, Y., Hu, J. L., Zhang, H. L. & Ying, Q. (2019), Source apportionment of summertime ozone in China using a source-oriented chemical transport model. Atmospheric Environment. 2019, 79–90. DOI: 10.1016/j.atmosenv.2019.05.006

Wang, T., Xue, L. K., Brimblecombe, P., Lam, Y. F., Li, L., & Zhang, L. (2017), Ozone pollution in China: A review of concentrations, meteorological influences, chemical precursors, and effects. Science of The Environment. https://doi.org/10.1016/j.scitotenv.2016.10.081

Wang, Y., Shen, L., Wu, S., Mickley, L., He, J., & Hao, J. (2013), Sensitivity of surface ozone over China to 2000–2050 global changes of climate and emissions. Atmospheric Environment, 2013, 75(4), 374–382. DOI: 10.1016/j.atmosenv.2013.04.045

Wei, W., Zhang, R. H., Wen, M., Rong, X. Y., & Li, T. (2014), Impact of Indian summer monsoon on the South Asian High and its influence on summer rainfall over China. Climate Dynamics, 2014, 1257–1269. DOI: 10.1007/s00382-013-1938-y

Xie, Y., Dai, H. C., Zhang, Y. X., Wu, Y. Z., Hanaoka, T., & Masui, T. (2019), Comparison of health and economic impacts of PM2.5 and ozone pollution in China. Environment International. DOI: 10.1016/j.envint.2019.05.075

Xu, X., Chen, W., & Chen, S. (2017), The climatology and interannual variability of the South Asia high and its relationship with ENSO in CMIP5 models. Climate Dynamics, 48.11–12,2017, 3507–3528. DOI: 10.1007/s00382-016-3281-6

Yin, Z. C., Cao, B. F., & Wang, H. J. (2019a), Dominant patterns of summer ozone pollution in eastern China and associated atmospheric circulations. Atmospheric Chemistry and Physics, 19(22), 13933–1394. DOI: 10.5194/acp-19-13933-2019

Yi in Arctic sea ice, Eurasian teleconnection pattern and summer surface ozone pollution in North China. Atmospheric Chemistry and Physics, 19(6), 3857–3871. DOI: 10.5194/acp-19-3857-2019

Yin, Z. C., Yuan, D. M., Zhang, X. Y., Yang, Q., & Xia, S. W. (2019c), Different Contributions of Arctic Sea Ice Anomalies from Different Regions to North China Summer Ozone Pollution, International Journal of Climatology, https://doi.org/10.1002/joc.6228

Yin, Z. C., Li, Y. Y., & Cao, B. F. (2020), Seasonal prediction of surface O3-related meteorological conditions in summer in North China, Atmospheric Research, https://doi.org/10.1016/j.atmosres.2020.105110

Zou, L. W., & Zhou, T. J. (2016), Future summer precipitation changes over cordex-east asia domain downscaled by a regional ocean-atmosphere coupled model: a comparison to the stand-alone rcm. Journal of Geophysical Research: Atmospheres, 2016, 121(6), 2691–2704. DOI: 10.1002/2015JD024519

Ta ...cal index.

	DTI	**V850pI-V850nI**	T200I
MDA8	0.52**	0.34**	-0.35**
	PI	T850I	
MDA8	-0.40**	0.30**	

All indices are normalized area averages of daily meteorological data. T850I, and T200I are temperature at 850 hPa (35°N-50°N, 110°E-120°E) and 200 hPa (35°N-50°N, 110°E-130°E), respectively. DTI is the normalized difference between T850 and T200. V850pI-V850nI is the normalized difference between the normalized area averaging meridional wind at 850 hPa over 32.5-42.5°N, 105-112.5°E and 40-50°N, 92.5-100°E. SSRI is downward surface solar radiation (35°N-45°N, 110°E-122.5°E). PI is total precipitation (37.5°N-42.5°N, 113°E-120°E). Indices in bold font were used to fit the model. '**' indicates a confidence level above 99%.

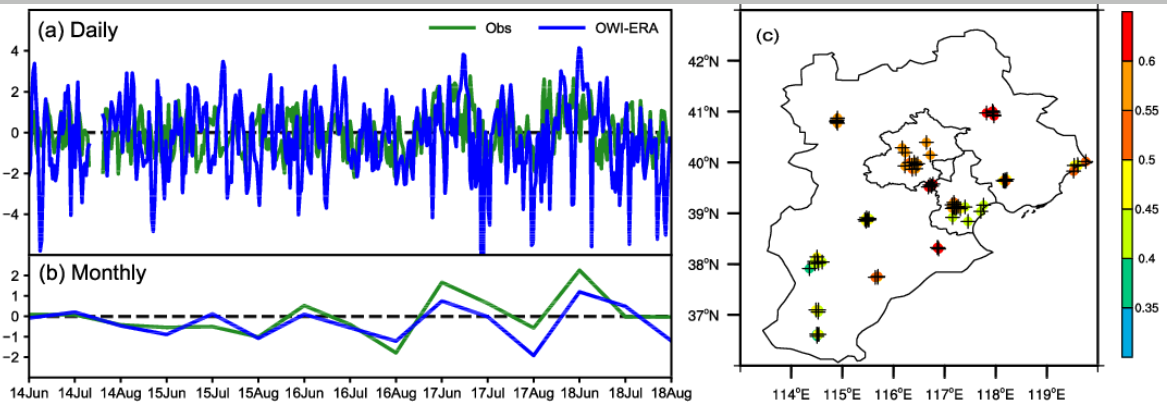

Figure 1. Variations in OWI and MDA8, and their correlations in observed sites. (a) Daily and (b) monthly observed MDA8 (green) and ERA-calculated OWI (blue). The dashed line indicates zero values. (c) Correlation coefficients between the daily OWI-ERA and MDA8 in Beijing-Tianjin-Hebei from 2014 to 2018. '+' indicates that the value is above the 99% confidence level. Panel (c) shows Beijing-Tianjin-Hebei region

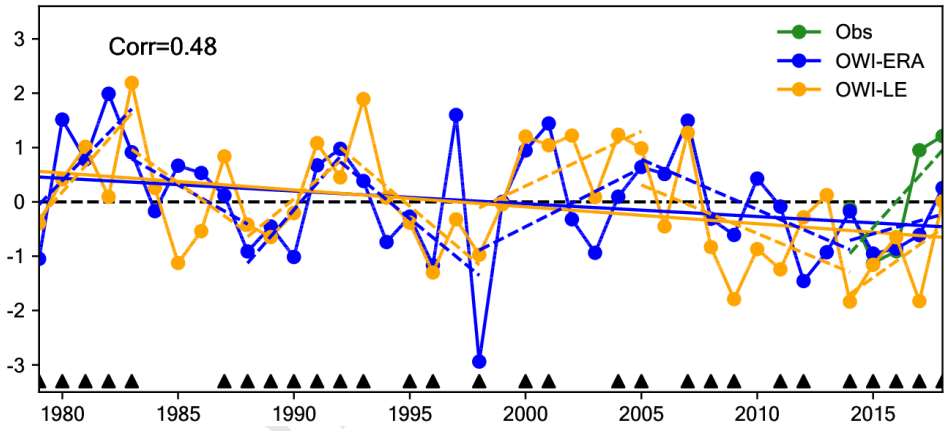

Figure 2. Standardized OWI-ERA (blue line), OWI-LE (orange line) during 1979-2018 and standardized BTH mean MDA8 (green line) during 2014-2018. Black triangles indicate that OWI-ERA and OWI-LE share the same mathematical symbol. Orange (OWI-LE), blue (OWI-ERA) and green (Obs) dashed lines are short-term trends. Long straight lines are the long-term trends of OWI-LE (orange) and OWI-ERA (blue) during 1979-2018. The dashed black line is the 0-line. 'Corr=0.48' is the correlation coefficient between the summer mean OWI-ERA and OWI-LE from 1979 to 2018.

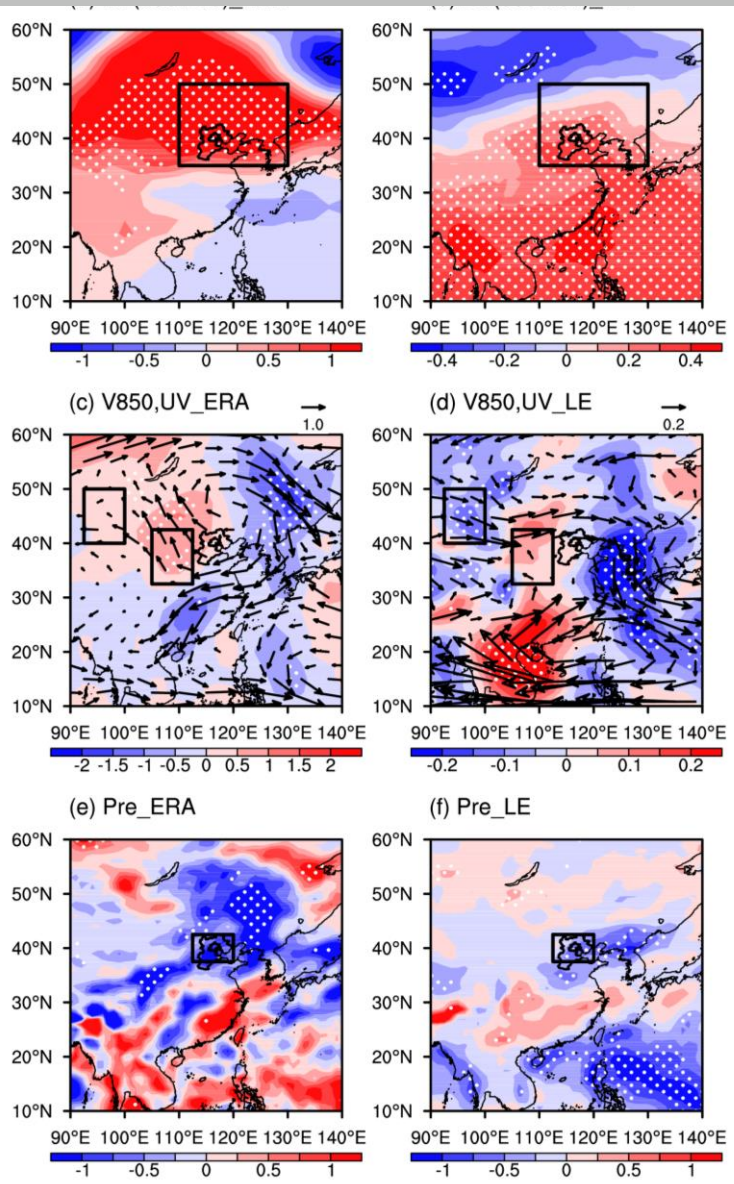

Figure 3. Composition of (a) (b) the temperature differences between 850 hPa and 200 hPa (shading), (c) (d) wind at 850 hPa (vector, shading is the meridional wind), and (e) (f) total precipitation (shading). The composite years were chosen by OWI-ERA, and OW-LE exceeded ±0.8 standard deviations. (a) (c) (e) Calculated from ERA-Interim and based on OWI-ERA. (b) (d) (f) Calculated from CESM-LE simulations and based on OWI-LE. The white dots denote that the CC was above the 95% confidence level. Black boxes indicate area used to calculate indices, (a) (b) for DT, (c) (d) for V850p and V850n, (e) (f) for precipitation.. Black irregular outlines show Beijing-Tianjin-Hebei region

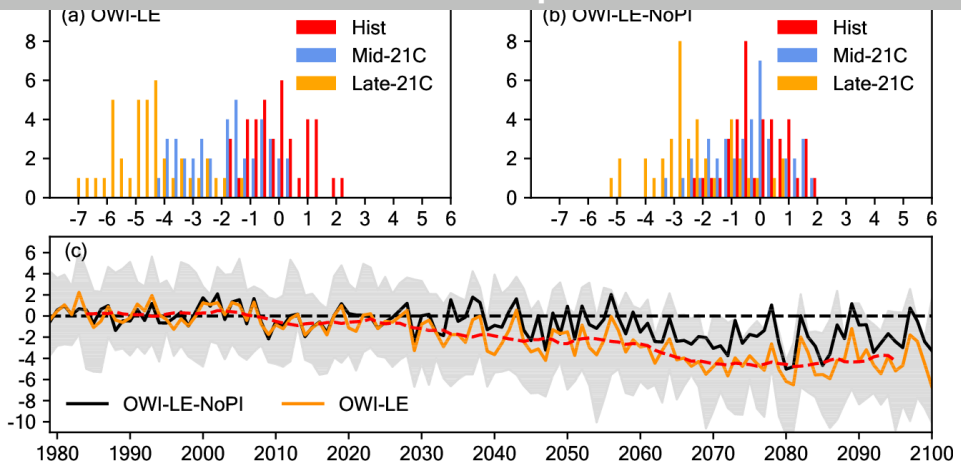

Figure 4. Frequency of (a) OWI-LE with PI and (b) without PI during 1979–2018 (red bar), Mid-21st century (2020–2059, blue bar), Late-21st century (2061~2100, orange bar). (c) Historical (1979-2018) and projected (2019-2100) OWI-LE with PI (orange solid line) and without PI (black solid line). The shadow ranges from the 75% to 25% quantiles. The dashed red line is the 11-year running average of OWI-LE with PI.

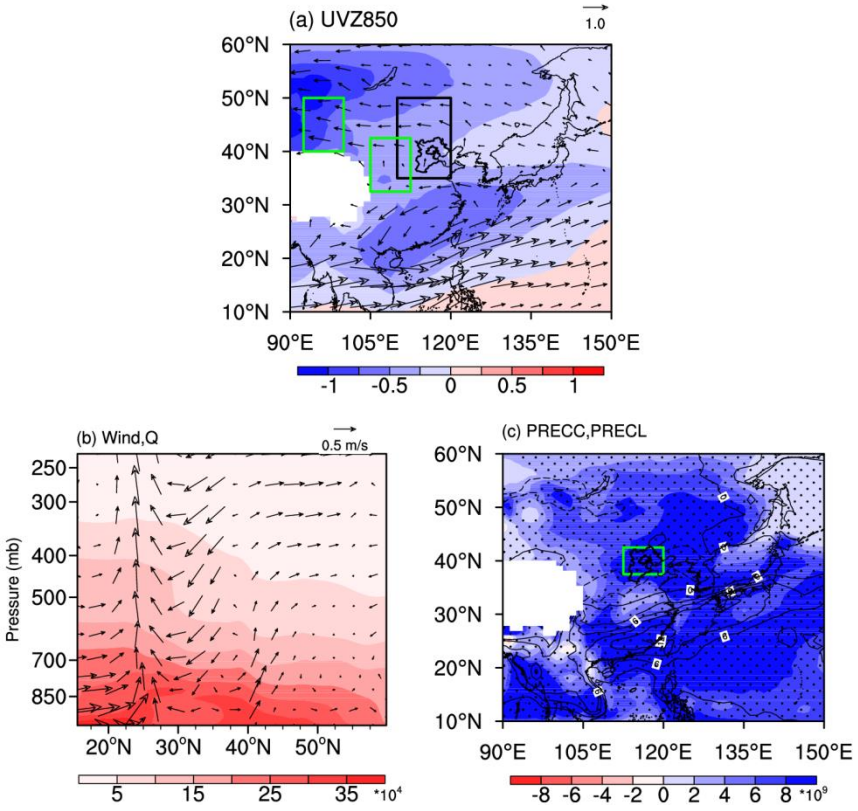

Figure 5. Difference between the mean of 2061-2100 and the mean of 1979-2018 (2061-2100 minus 1979-2018) for (a) the temperature difference between 850 hPa and 200 hPa (shading) and wind at 850 hPa (arrows), (b) 113°-117°E mean latitude–high wind (arrows) and specific humidity (shading) and (c) convectional precipitation (shading) and large-scale precipitation (contour). Black dots in panel c indicate that the value of total precipitation (convectional + large-scale precipitation) is positive. Boxes indicate area used to calculate indices, (a) black boxes for T850, green boxes for V850p and V850n and (c) for precipitation. Black irregular outlines show Beijing-Tianjin-Hebei area.

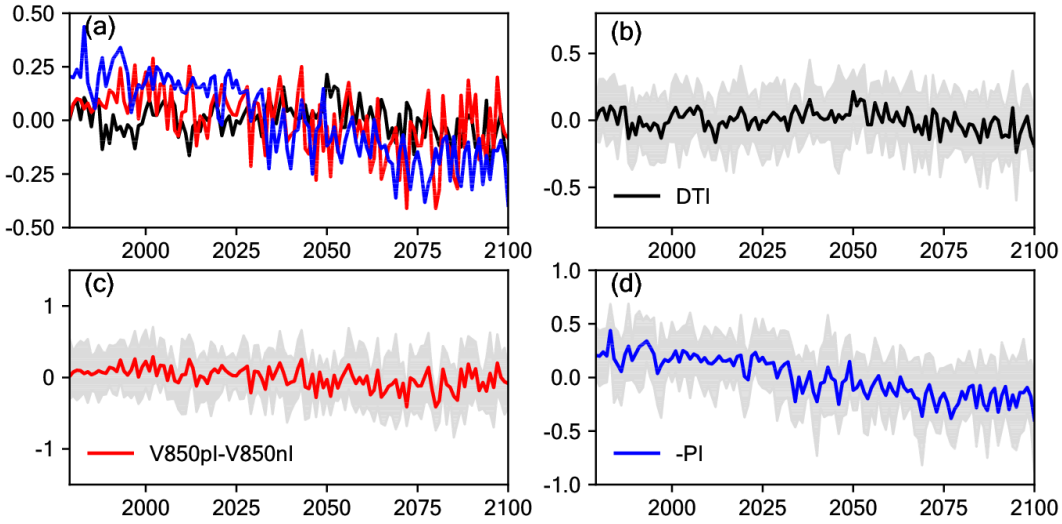

Figure 6. (a) Variation in the temperature difference between 850 hPa and 200 hPa (black line), difference between V850pI and V850nI (red line) and –PI (blue line); (b) variation in the temperature difference between 850 hPa and 200 hPa; (c) variation in the difference between V850pI and V850nI; (d) variation in –PI. The shadowed areas are for the ranges from the 75% to 25% quantiles for the indices calculated from all CESM-LE simulations.

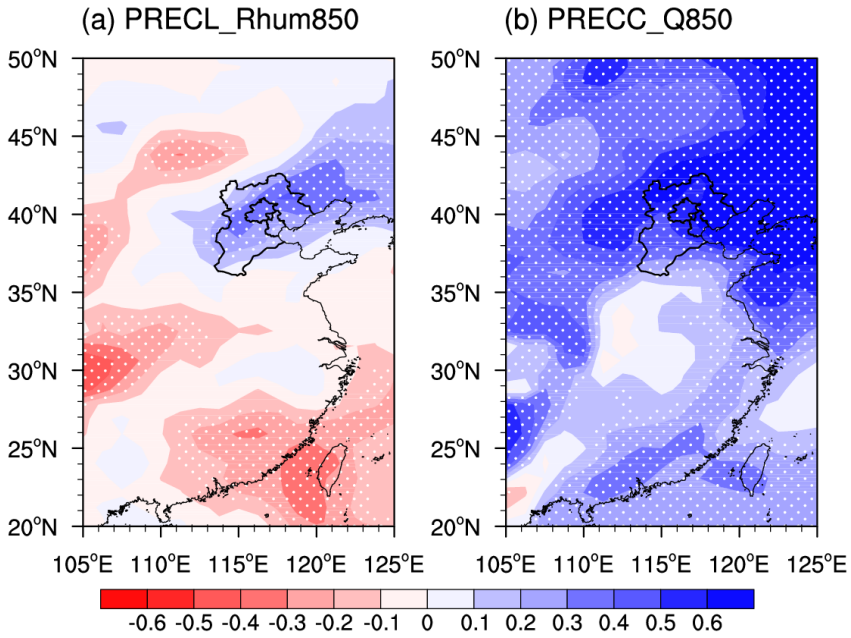

Figure 7. Correlation coefficients between (a) large-scale precipitation and relative humidity and (b) those between convectional precipitation and specific humidity during 1979 to 2100. The linear trend was removed. Black irregular outlines show Beijing-Tianjin-Hebei area.

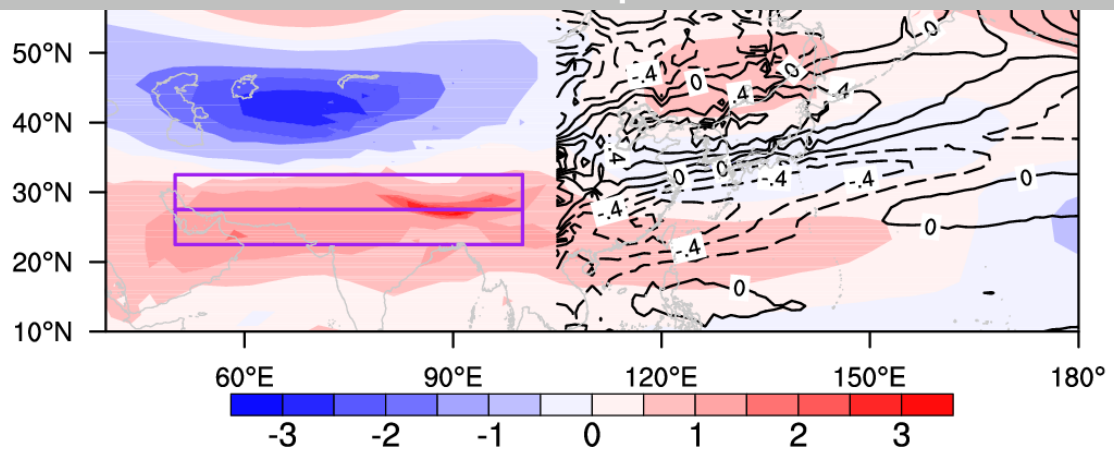

Figure 8. Difference between the mean of 2061-2100 and the mean of 1979-2018 (2061-2100 minus 1979-2018) for the eddy geopotential height at 100 hPa (shading) and at 500 hPa (counter). Purple boxes indicate the area used to calculate I_{ns}.

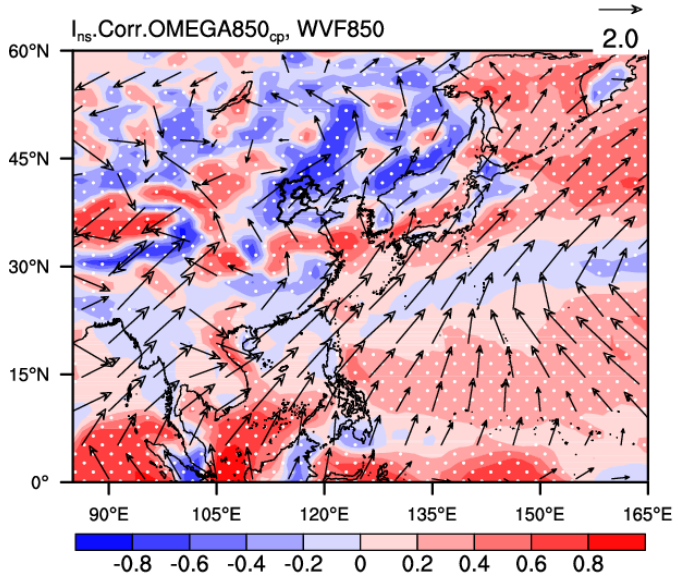

Figure 9. Correlation coefficients between -1xI_{ns} and water vapour flux at 850 hPa (vector) and omega (subtracting the omega regressed on large-scale precipitation) at 850 hPa (shading). White dots indicate that the correlation coefficients between -1xI_{ns} and omega are above the 95% confidence level. Black irregular outlines show Beijing-Tianjin-Hebei area.

Bu ng,

Visualization

Zhicong Yin: Conceptualization, Project administration, Funding acquisition. Writing - Review & Editing

☒ The authors declare that they have no known competing financial interests or personal relationships that could have appeared to influence the work reported in this paper.

☐The authors declare the following financial interests/personal relationships which may be considered as potential competing interests:

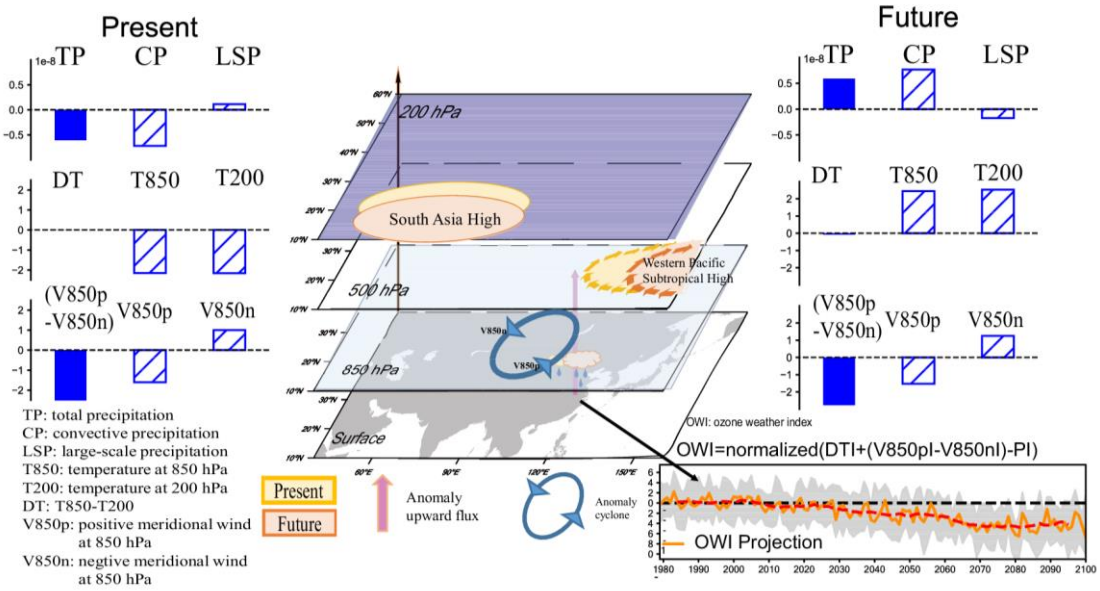

Graphical abstract

- Ozone weather index was established which can effectively extract climate anomalies affecting ozone from climate simulations.
- Atmospheric circulation will favour the control of ozone pollution in the Beijing-Tianjin-Hebei region.
- Changes in moisture and dynamics with global warming lead to increasing convective precipitation that weakens surface ozone.